

## Elasticity-Dependent Self-assembly of Micro-Templated Chromonic Liquid Crystal Films: Supplemental Material

M. A. Lohr<sup>1</sup>, M. Cavallaro Jr.<sup>2</sup>, D. A. Beller<sup>1</sup>, K. J. Stebe<sup>2</sup>, R. D. Kamien<sup>1</sup>, P. J. Collings<sup>1,3</sup>, A. G. Yodh<sup>1</sup>

<sup>1</sup>*Department of Physics and Astronomy, University of Pennsylvania, Philadelphia, PA 19104, USA*

<sup>2</sup>*Department of Biomolecular and Chemical Engineering,*

*University of Pennsylvania, Philadelphia, PA 19104, USA and*

<sup>3</sup>*Department of Physics and Astronomy, Swarthmore College, Swarthmore, PA 19081, USA*

(Dated: December 20, 2013)

### I. POST TRACKING, ROTATION REMOVAL, AND DIRECTOR FIELD QUANTIFICATION

Birefringent lyotropic chromonic liquid crystal (LCLC) films in micropost arrays are placed on a rotating stage of a Leica DM IRB microscope under a 63x air objective between cross polarizers. Once the stage is centered to ensure that the center of rotation lies in the microscope field of view, the stage is rotated by hand a total of 360° while video is acquired at 10 frames per second on an UNIQ UP 680-CL digital camera. The resulting images have a resolution of 312 nm/pixel. The polarizer and analyzer direction in the resulting video are fixed on the image's vertical and horizontal axes.

To track the translation and rotation of the sample, we process the images to make post locations trackable via well-used particle tracking algorithms. Specifically, we invert the image (Figure 2), raise the contrast by raising the pixel intensity to the eighth power, then convolute it with the image of a bright disk with a radius equal to the observed post radius in the images (Figure 3). After setting all pixels below an arbitrary threshold to zero, this gives us a set of bright intensity peaks located at the centers of posts. We then track the bright intensity peaks using a commonly used sub-pixel tracking algorithm [1]. The tracked post locations compare well with the original unprocessed image (Figure 4).

The resulting tracks yield important information about the motion of the sample during rotation between cross-polarizers. We first calculate the average motion of all tracked posts from frame to frame; this yields translational motion of the sample due to slight shifts in the stage during manual rotation. We remove this frame-to-frame motion from the video using a cubic convolution interpolation method. This yields a video with pure rotational motion (Figure 5).

The rotation of the system from frame  $t$  to  $t+1$  is calculated as the average rotation angle  $\theta_i(t)$  of each post position  $(x_i, y_i)$  around the mean post position  $(x_0, y_0)$ , given the motion of each post  $\mathbf{dr}_i(\mathbf{t}) = (\mathbf{x}_i(\mathbf{t} + 1) - \mathbf{x}_i(\mathbf{t}), \mathbf{y}_i(\mathbf{t} + 1) - \mathbf{y}_i(\mathbf{t}))$ ,  $r_i(t) = x_i(t) - x_0, y_i(t) - y_0$ , and  $dr_{perp}$ , the component of  $dr$  perpendicular to  $r$ , given the approximation  $\theta_i = dr_{perp}/r$ . We take this approximation as valid, since the rotation of the system over a single time frame is no greater than 3°. The rotation  $\theta(t)$  is then removed from the original, unprocessed images using a cubic convolution interpolation. The resulting video shows stationary posts as the polarizer and analyzer are rotated at an angle  $\theta_{pol} = -\theta_{sample}$  to the vertical/horizontal directions in the images (Figure 6).

The equation for transmitted light intensity of a birefringent liquid crystal sample between cross-polarizers is given by

$$I_t = I_i \sin^2(\phi/2) \sin^2(2\theta), \quad (1)$$

where  $\theta$  is the angle between the optical axis of the liquid crystal (director) and the polarizer/analyzer. The retardation  $\phi$  depends on the sample thickness, birefringence, and out-of-plane tilt angle. Assuming the director is in the plane, the term containing  $\phi$  does not vary spatially, so the relative intensity should depend only on the term containing  $\theta$ . Thus we consider the intensity variations per pixel as the polarizer and analyzer are rotated with respect to the LCLC film as

$$I_t = I_0 \sin^2(2(\theta_{dir} - \theta_{pol})), \quad (2)$$

where  $I_0$  is a qualitative measure of the in-plane director order (a small value indicates a locally disordered defect, or a director oriented out-of-plane). Indeed, by looking at representative pixels intensities in a motion-removed image, we see this functional form fits well (Figure 7). Thus, by fitting curves to Eq. (2), with  $I_0$  set as the amplitude of intensity fluctuations, we find the average in-plane director angle  $\theta_{dir}$  at each pixel.

There exists a degeneracy in this fitting method for finding  $\theta_{dir}$ , since  $I_0 \sin^2(2(\theta_{dir} - \theta_{pol})) = I_0 \sin^2(2((\theta_{dir} + \pi/2) - \theta_{pol}))$ . However, we determine whether local director orientation follows  $\theta_{dir}$  or  $\theta_{dir} \pm \pi/2$  by comparing images with full-waveplate retardation cross-polarizer images (which distinguishes local directors under  $\pi/2$  rotations), observing

local post boundary conditions (directors should lie parallel to post surfaces in minimum-energy configurations), and minimizing obvious director discontinuities.

[1] J. C. Crocker and D. G. Grier, *J. Colloid Interface Sci.* **179**, 298 (1996).

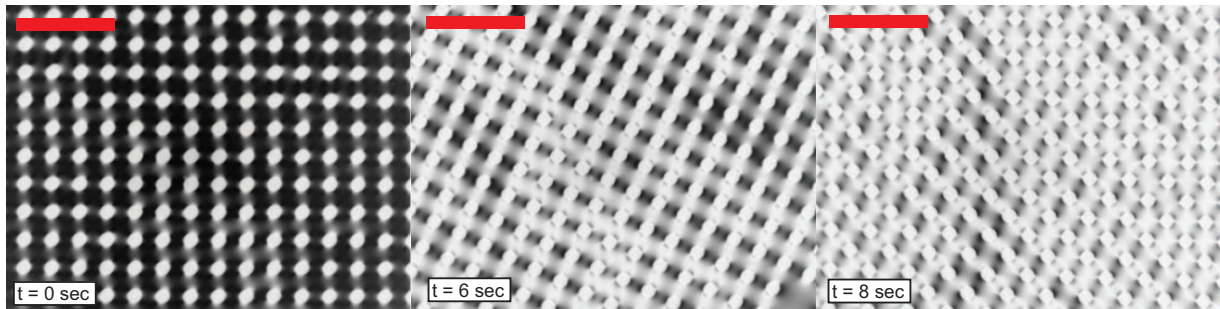


FIG. 2: Inverted images from rotating SSY movie shown in Figure 1. Scale bar =  $50 \mu\text{m}$ .

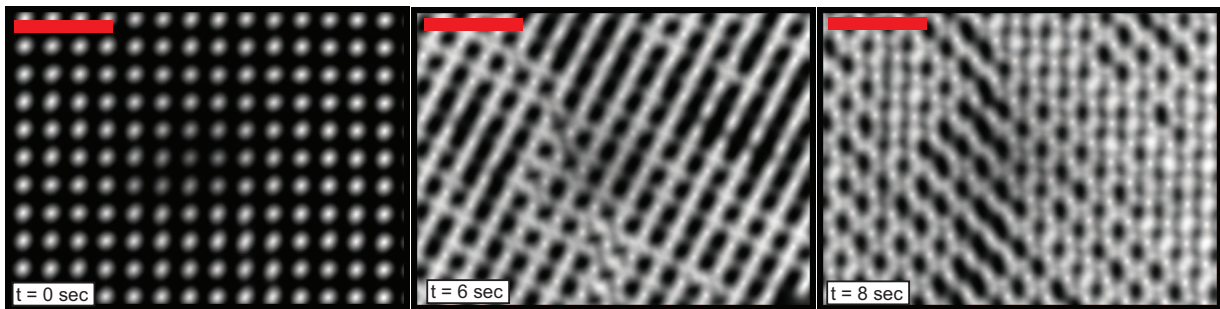


FIG. 3: Inverted images from rotating SSY movie convoluted with a uniformly bright disk of diameter equal to the post diameter. Scale bar =  $50 \mu\text{m}$ .

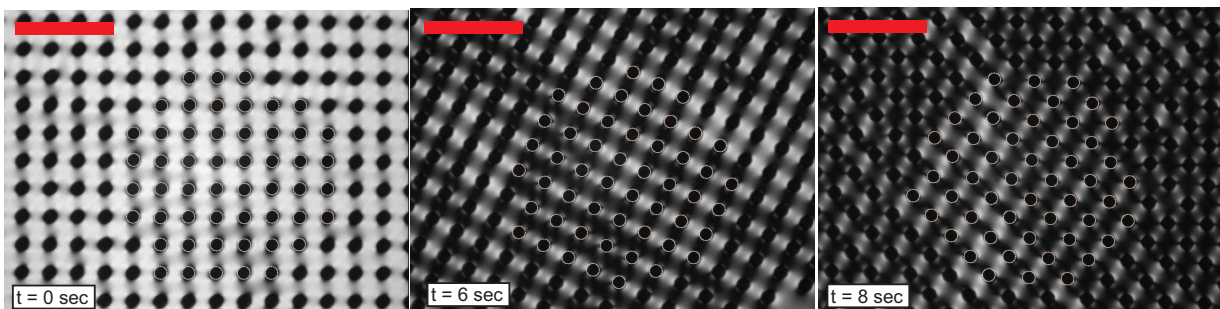


FIG. 4: Original cross-polarizer images of rotating SSY film, overlaid with bright circles centered at tracked post centroids. Scale bar =  $50 \mu\text{m}$ .

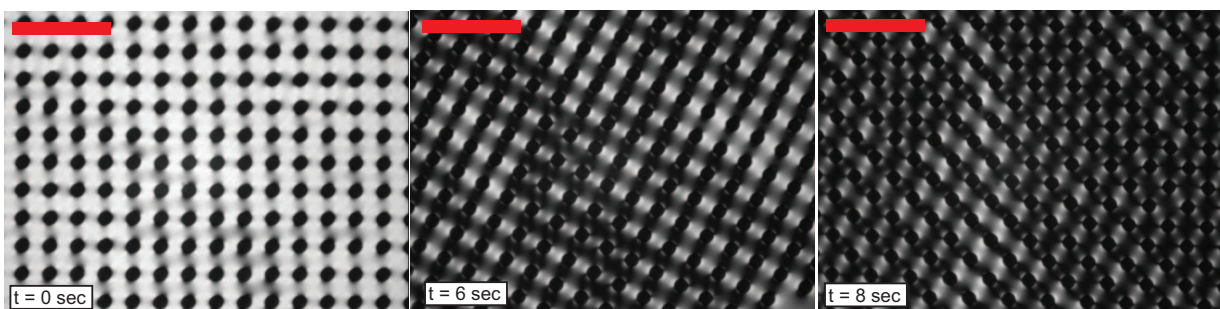


FIG. 1: Cross-polarizer images from a movie of a rotating 30 percent Sunset Yellow aqueous nematic film in an array of cylindrical microposts of diameter  $7 \mu\text{m}$  and height  $5 \mu\text{m}$ . Polarizer and analyzer oriented along the vertical and horizontal of images. Scale bars =  $50 \mu\text{m}$ .

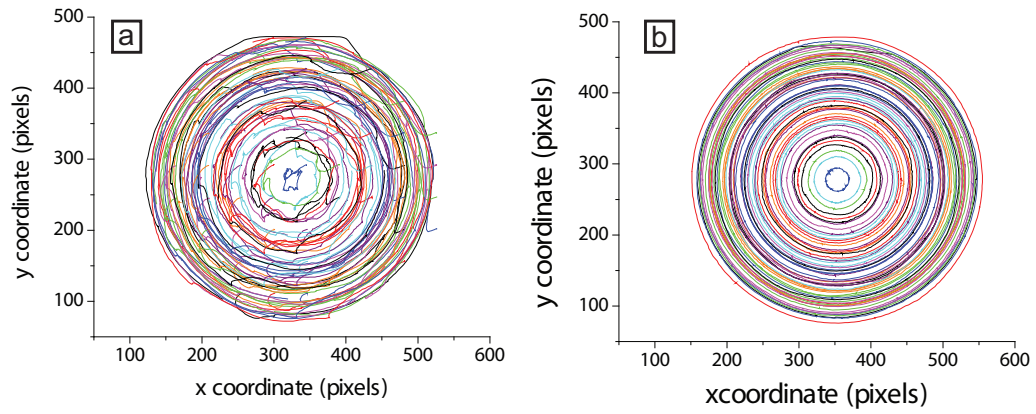


FIG. 5: (a) Trajectories of 59 posts tracked through a  $360^\circ$  sample rotation. (b) Trajectories with average translational motion per frame removed.

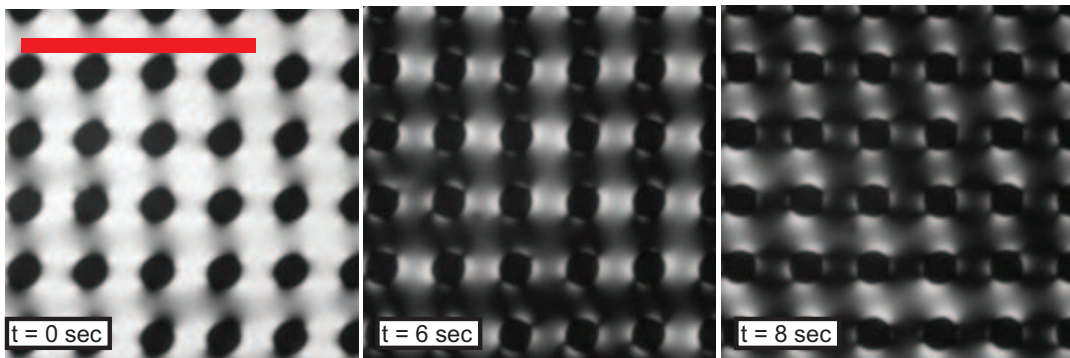


FIG. 6: Selections of images of the SSY film from Figure 1, with net sample rotation and translation removed. Polarizer/analyzer are oriented at angles of  $0^\circ$  ( $t = 0$  sec),  $37^\circ$  ( $t = 6$  sec), and  $55^\circ$  ( $t = 8$  sec) with respect to the vertical/horizontal of images.

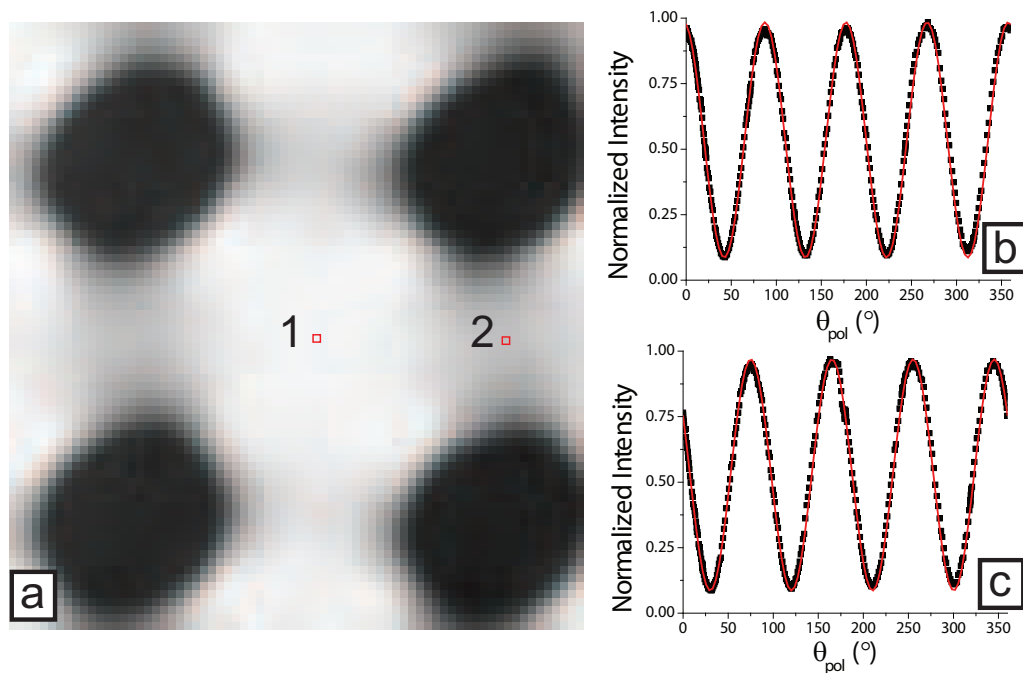


FIG. 7: (a) Selection of unprocessed video of SSY film under cross-polarizers, when the polarizer/analyzer is oriented at an angle of  $0^\circ$  ( $t = 0$  sec) with respect to the vertical/horizontal of the image. (b-c) Image brightness / transmitted light intensity at pixels 1 and 2, respectively, as a function of the angle of polarizer/analyzer to image horizontal/vertical,  $\theta_{dir}$ . Red lines indicate fits to the function  $I = I_0 \sin^2(2(\theta_{dir} - \theta_{pol})) + B$ , where  $I_0$  is the difference in maximum and minimum intensity, and  $B$  is the minimum intensity value. For (a),  $\theta_{dir} = 42.3^\circ$ , and (b),  $\theta_{dir} = 30.15^\circ$ .

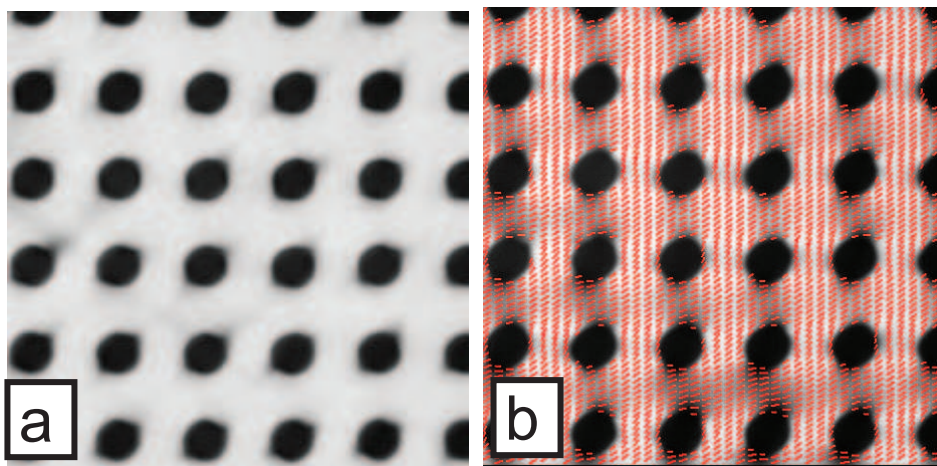


FIG. 8: (a) Relative in-plane director magnitude,  $I_0$ . As discussed in the paper, indications of defects at the diagonal ends of posts are shown as small dark spots. (b) In-plane director orientation (red lines) plotted over grayscale image of in-plane director magnitude  $I_0$ . For the sake of clarity, only every 10th pixel is represented in this image.